Kineococcus radiotolerans Dps forms a heteronuclear Mn–Fe ferroxidase center that may explain the Mn-dependent protection against oxidative stress

Matteo Ardini [a,1], Annarita Fiorillo [a,1], Maria Fittipaldi [c], Simonetta Stefanini [a], Dante Gatteschi [c], Andrea Ilari [b], Emilia Chiancone [a,b,*]

[a] Department of Biochemical Sciences "A. Rossi Fanelli", "Sapienza" University of Rome, Pl. A. Moro 5, 00185, Italy
[b] CNR Institute of Molecular Biology and Pathology, Pl. A. Moro 5, 00185 Rome, Italy
[c] Department of Chemistry, University of Florence, Via della Lastruccia 3, 50019 Sesto Fiorentino (Fi), Italy

ABSTRACT

Background: The ferroxidase center of DNA-binding protein from starved cells (Dps) is a major player in the iron oxidation/detoxification process that leads to a decreased reactive oxygen species production. The possible Mn(II) participation in this process has been studied in Dps from Kineococcus radiotolerans, a radiation-resistant bacterium with a high cytosolic Mn/Fe ratio and a high capacity to survive ionizing and stress conditions.
Methods: The X-ray structure of recombinant K. radiotolerans Dps loaded with Mn(II) has been solved at 2.0 Å resolution. Mn(II) binding to K. radiotolerans Dps and its effect on Fe(II) oxidation have been characterized in spectroscopic measurements.
Results: In K. radiotolerans Dps, the Fe–Fe ferroxidase center can have a Mn–Fe composition. Mn(II) binds only at the high affinity, so-called A site, whereas Fe(II) binds also at the low affinity, so-called B site. The Mn–Fe and Fe–Fe centers behave distinctly upon iron oxidation by O_2. A site-bound Mn(II) or Fe(II) plays a catalytic role, while B site-bound Fe(II) behaves like a substrate and can be replaced by another Fe(II) after oxidation. When H_2O_2 is the Fe(II) oxidant, single electrons are transferred to aromatic residues near the ferroxidase center and give rise to intra-protein radicals thereby limiting OH⁺ release in solution. The presence of the Mn–Fe center results in significant differences in the development of such intra-protein radicals.
Conclusions: Mn(II) bound at the Dps ferroxidase center A site undergoes redox cycling provided the B site contains Fe.
General significance: The results provide a likely molecular mechanism for the protective role of Mn(II) under oxidative stress conditions as it participates in redox cycling in the hetero-binuclear ferroxidase center.

© 2013 Elsevier B.V. All rights reserved.

1. Introduction

The protective role played by Mn in bacteria under several growth conditions that lead to oxidative stress and the correlations that link Mn and Fe, another essential metal, are known since many years. However, the underlying molecular mechanisms are still not fully understood [1]. Lactobacillus plantarum is an aerotolerant bacterium which grows on fermenting Mn-rich plant material and accumulates this metal up to millimolar concentrations. The ability of this bacterium to tolerate oxygen exposure despite the lack of superoxide dismutase was ascribed to the spontaneous formation of Mn(II) complexes with small cellular ligands, like phosphate and lactate, which

act in vitro as superoxide or hydrogen peroxide scavengers [2,3]. This contention was supported by the observation that in Staphylococcus aureus Mn(II) forms a complex with lactate and orthophosphate and that the metal oxidation state in such complexes is influenced by oxygenation of the cell [4,5].

The linkage between Mn and Fe, which is key to the present work, was established in later studies on the regulation of Mn transport. In brief, the uptake of both metals is controlled by members of the ferric uptake regulator (Fur) and DtxR family which act as Fe(II)- and Mn(II)-dependent transcriptional repressors, respectively [6,7]. In S. aureus and Escherichia coli, for example, the DtxR-like Mn(II) transporter, MntR, reduces transcription when the cellular Mn concentration is high. Interestingly, Mn(II) transport via MntR is controlled also by OxyR, in E. coli, and PerR, in S. aureus, which afford peroxide resistance and hence link Mn(II) transport to the level of reactive oxygen species (ROS) in the cell. In recent work on E. coli, the relevant Mn(II) transporter, MntH, was found to support the growth of iron-deficient cells and to be induced strongly upon H_2O_2 stress [8].

Mn was suggested to substitute Fe in some key metalloenzymes to account for the fact that, in contrast to current belief, Mn does not protect peroxide-stressed cells by scavenging H_2O_2. Among the possible candidates, the Dps protein was mentioned, a shell-like 12mer of the ferritin family that is induced during H_2O_2 stress and catalyzes Fe(II) oxidation at the ferroxidase center. Like all such centers, the Dps protein ferroxidase center is binuclear and typically binds two Fe ions with different affinities. Subsequently, oxidized iron is sequestered in the protein cavity thereby inhibiting the Fenton-mediated production of ROS [9,10]. The possible substitution of Fe by Mn at the ferroxidase-center was not investigated even though Dps was suggested to be involved in the protection of peroxide-stressed cells since Mn supplementation of the growth medium suppresses the marked growth defect of mutants lacking Dps, peroxidase and catalase [8].

These data inspired the present work which establishes for the first time that Mn binds at the ferroxidase center of *Kineococcus radiotolerans* Dps (*Kr*Dps) and that this ion undergoes redox cycling just as Fe. The choice of the system was suggested by the work of Daly and collaborators on the unusual γ radiation-resistant bacterium *Deinococcus radiodurans* [11,12]. The *D. radiodurans* cytoplasm is characterized by high Mn concentrations and by low Fe levels such that the intracellular Mn/Fe ratio is significantly larger than in radiation-sensitive bacteria (0.24 compared to 0.0072 in *E. coli*). In line with this finding, when Mn availability in the growth medium is limited, and hence active Mn transport and accumulation impaired, radiation-resistance is drastically decreased [11]. These observations, and the fact that the harmful effects of radiations are mediated primarily by ROS, led us to the same suggestion put forward by Archibald and Fridovich [2,3], namely that Mn prevents the iron-dependent ROS development by the spontaneous formation of complexes with small cellular ligands which act as catalytic ROS scavengers [12], a contention challenged by the work of Anjem et al. [8] just mentioned.

K. radiotolerans is a radiation-resistant bacterium and is characterized by a high cellular Mn concentration and a high Mn/Fe ratio, just like *D. radiodurans*. The data presented here show that Mn(II) binds at the high affinity A site but not at the low affinity B site of the binuclear ferroxidase center of *Kr*Dps, whereas Fe(II) can bind at both the A and B sites. Importantly, the experiments unveiled that A site-bound Mn(II) has a catalytic role and participates in the ferroxidation reaction, whereas B site-bound Fe(II) acts as a substrate and, after each ferroxidation cycle, can be displaced by another Fe(II).

The present findings are discussed also in the framework of recent discoveries on the formation of Mn–Fe hetero-nuclear cofactors in *Chlamydia trachomatis* ribonucleotide reductase [13] and in the Dps-like protein of *Sulfolobus solfataricus* [14] whose catalytic centers closely resemble those of *Kr*Dps.

2. Materials and methods

2.1. Protein preparation

A pET-11a vector plasmid (5600 bp) containing the *Krad_4280* wild-type gene (513 bp) was purchased from GeneArt AG (Germany) and introduced into *E. coli* BL21 (DE3) competent cells (Invitrogen) by heat shock transformation. After protein induction, purification was carried out following the procedure described for *Listeria innocua* Dps (*Li*Dps) [15] which comprises a heat shock step (8 min at 348 K) followed by precipitation in ammonium sulfate (60% w/v) and further purification by ion-exchange chromatography.

All buffers used for *K. radiotolerans* (*Kr*Dps) purification contained 200 mM NaCl to avoid protein self-aggregation. Protein concentration, expressed on a 12mer basis throughout, was determined spectrophotometrically at 280 nm using the molar extinction coefficients 1.98×10^5 M^{-1} cm^{-1} for *Kr*Dps and 2.03×10^5 M^{-1} cm^{-1} for *Li*Dps [16] on the basis of a 12mer molecular mass of 224.5 kDa and 216 kDa, respectively. The metal content of the purified proteins,

assessed by atomic absorption spectroscopy, was ≤0.55 Fe/12mer and ≤0.02 Mn/12mer for *Kr*Dps and 1.2 Fe/12mer and 0.02 Mn(II)/12mer for *Li*Dps. Unless otherwise stated, all experiments were carried out in 50 mM MOPS–NaOH buffer, pH 7.4 containing 200 mM NaCl.

The site-specific mutant *Kr*Dps(W56F), where Trp56 is mutated into Phe, namely the residue present in most Dps proteins, was obtained by means of the QuikChange Site-Directed Mutagenesis Kit (Stratagene). The mutagenesis procedure was made on the pET-11a plasmid containing the wt *Kr*Dps gene using the forward and reverse primers 5′-GGAACATTGTGGGCGAAAACTTCCGCGATCTGCATCTGCAGC TGG-3′ and 5′-CAGCTGCAGATGCAGATCGCGGAAGTTTTCGCCCACAAT GTTCC-3′, respectively. The construct was sequenced to confirm sequence integrity. *Kr*Dps(W56F) was purified as described for *Kr*Dps. The *Kr*Dps(W56F) concentration was calculated using the molar extinction coefficient of 1.32×10^5 M^{-1} cm^{-1} on the basis of a 12mer molecular mass of 224.5 kDa.

2.2. Protein crystallization, data collection and data processing

Crystallization experiments, carried out at 298 K by the hanging drop vapor diffusion method, yielded X-ray quality crystals in one week. For the crystallization trials, 24 Mn(II)/12mer were added to *Kr*Dps at ~10 mg/ml (44 μM). After dialysis against 20 mM Tris–HCl at pH 7.5, aliquots of the protein solution were mixed with an equal amount of reservoir solution containing 45% v/v MPD (2-methyl-2,4-pentanediol) and 0.1 M Tris–HCl at pH 8.0. Well shaped crystals grew in one week and reached dimensions of $0.3 \times 0.2 \times 0.2$ mm^3. Crystals were mounted in nylon loops and flash-frozen by quick submersion into liquid N_2 for transport to the synchrotron. Two single wavelength data sets ($\lambda = 0.918$ Å) were collected at 100 K from two *Kr*Dps crystals at the synchrotron radiation source in BESSY, Berlin, Germany, using a MAR 225 CCD detector. The data sets were processed separately with DENZO and scaled together with SCALEPACK [17]. The auto-indexing procedure indicates that crystals are rhombohedral. Based on the scaling procedure, crystals belong to the R3 space group with cell parameters: a = b = 150.47 Å, c = 86.62 Å and α = β = 90°, γ = 120°. The data are 100% complete with an R_{merge} value of 8.3% at 2.0 Å resolution. The data statistics are reported in Table 1.

Table 1
Crystal parameters, data-collection and refinement statistics of *Kr*Dps. Values in parentheses are for the highest resolution shell.

Crystal parameters and data scaling	
Space group	R3
Unit-cell parameters	
a (Å)	150.47
b (Å)	150.47
c (Å)	86.61
No. of monomers in ASU	4
<B> for atomic model ($Å^2$)	16.2
Resolution ranges (Å)	2.0–50.0 (2.0–2.07)
Unique reflections	49,300 (4946)
Completeness (%)	100 (100)
Redundancy	16.7 (14.6)
R_{merge}[a] (%)	8.3 (33.9)
χ^2[b]	1.098 (0.83)
<I/s(I)>	40.95 (7.77)

Refinement and geometric parameters	
Resolution ranges (Å)	2.0–50.0 (2.0–2.05)
R_{crys} (%)	19.61
R_{free} (%)	23.22
RMS (angles)	1.15
RMS (bonds)	0.01
Residues in core region of Ramachandran plot	96.1%
Residues in allowed region of Ramachandran plot	3.9%

[a] $R_{merge} = S_{hkl}S_i |I_i(hkl) - <I(hkl)>|/S_{hkl}S_i I_i(hkl)$ where $I_i(hkl)$ is the observation of the reflection (hkl) and <I(hkl)> is the mean intensity of the (hkl) reflection.
[b] $\chi^2 = S_{ii} (|I_{ij}(hkl) - <I_i(hkl)>|)^2/(s_i^2 N/(N-1))$.

2.3. Structure solution and refinement

The *Kr*Dps structure was solved by molecular replacement using as search model *Mycobacterium smegmatis* Dps 2 (*Ms*Dps2, PDB ID: 2Z90) since it displays 56% sequence identity with *Kr*Dps (calculated using the NCBI-BLAST server). The rotational and translational searches performed with MOLREP in the resolution range 10.0–3.0 Å produced a clear solution [18].

Refinement was performed using the maximum likelihood method with the program REFMAC including individual isotropic B-factor and TLS refinement [19], while model building was performed with the program COOT according to Emsley and Cowtan [20]. The final *Kr*Dps model is a tetramer containing 668 residues (167 residues for chain A, 169 residues for chains B and C and 166 residues for chain D), 10 Mn(II) ions (4 with full, 2 with 0.7, 1 with 0.5, 2 with 0.33, 1 with 0.15 occupancy), 6 chloride ions (5 with full and 1 with 0.33 occupancy) and 322 water molecules. The final R_{crys} for all resolution shells (50–2.0 Å) calculated using all 46,797 reflections is 19.6%, and the free R value calculated using the 2491 test set reflections is 23.2%. The final R_{crys} calculated for the highest resolution shell (2.05–2.0 Å) using the working set reflections (3411) is 23.9%, and the free R value calculated using the test set reflections (203) is 29.0%. The most favored regions of the Ramachandran plot contain 96.1% of the residues (Table 1).

The metal ions bound to the protein were identified by means of X-ray fluorescence emission spectra collected at the BESSY synchrotron radiation source (Beamline BL-14.1) in an energy range between 2000 and 25,000 eV.

2.4. Fe(II) and Mn(II) binding: anaerobic fluorescence titrations

Fe(II) and Mn(II) binding to *Kr*Dps was followed by measuring the intrinsic protein fluorescence under anaerobiosis using a Fluoromax-4 spectrofluorometer (Horiba-Jobin Yvon). The excitation wavelength was 290 nm, emission was recorded between 300 and 400 nm using 5 nm entry and exit slits. All measurements were carried out at 298 K under a N_2 atmosphere in a gas tight, 1 cm path length cell under continuous stirring. Metals were added to a 2 μM apo-*Kr*Dps protein solution in 4 ions/12mer increments. Fe(II) was added as an anaerobic 2.4 mM Fe(NH$_4$)$_2$SO$_4$ solution in 1 mM HCl. Mn(II) was prepared as an anaerobic 2.4 mM solution in distilled water obtained by dilution of a standard solution (Fluka).

2.5. Kinetics of Fe(II) oxidation by O₂: spectrophotometric assays

The kinetics of Fe(II) oxidation by O_2 was assessed spectrophotometrically on a 8452A Diode Array spectrophotometer (Hewlett–Packard). Fe oxidation was followed for 60 min by measuring the ferric hydrous oxide formed at 310 nm. The amount of oxidized iron was calculated using the molar extinction coefficient, $E_{M, 310 nm} = 2528$ M^{-1} cm^{-1}, reported in Ref. [15]. All experiments were performed at 298 K in a 1 cm path length cell on 6 μM *Kr*Dps maintained under continuous stirring in air. Mn(II), when present, was added to the protein solution 5 min before Fe(II) addition. Fe(II) and Mn(II) were prepared as 37.7 mM solutions as described for the fluorescence experiments. The data were analyzed with Origin 8 PRO software (OriginLab, Northampton, MA, USA).

2.6. Kinetics of Fe(II) oxidation by H₂O₂: stopped-flow experiments

Generation of transient intra-protein radical species upon oxidation of Fe(II) by H_2O_2 and the possible effect of Mn(II) were assessed in a stopped-flow apparatus equipped with a Spectra/kinetic monochromator (Applied PhotoPhysics). Experiments were performed at 298 K in a sequential mixing setup by recording absorbance spectra in the diode array mode between 350 and 700 nm every 3 ms for a total of 300 ms. A 68 μM protein solution in 200 mM MOPS–NaOH,

pH 7.4 containing 800 mM NaCl was mixed with 400 μM FeSO$_4$ in 1 mM HCl and, after a 500 ms delay, with 100 μM H_2O_2 to obtain a final reaction mixture with a molar ratio of 6 Fe(II)/12mer and 3 H_2O_2/12mer. A second set of experiments was performed using a protein solution pre-loaded with 12 Mn(II)/12mer. For these experiments, MnCl$_2$ was dissolved freshly in distilled water. In a third set, the protein solution was mixed with 800 μM MnCl$_2$ and, after a 500 ms delay, with 100 μM H_2O_2 to achieve a molar ratio of 12 Mn(II)/6 H_2O_2/12mer. The data were analyzed with Origin 8 PRO (OriginLab, Northampton, MA, USA). To calculate the yield of tryptophan radical species the published molar coefficient extinction of 2300 ± 150 M^{-1} cm^{-1} was used [21].

2.7. Sedimentation velocity experiments

Sedimentation velocity experiments were carried out at 30,000 rpm and 293 K on a Beckman XLI analytical ultracentrifuge using absorbance optics. The experiments were conducted on a 4 μM apo-*Kr*Dps solutions pre-soaked for 2 h with 240 Mn(II) or 240 Fe(II)/12mer in air or in the presence of H_2O_2 (0.5 equivalents relative to the metal). Radial absorbance scans were obtained at a spacing of 1.2 cm in a continuous scan mode; 3 subsequent scans were averaged. Sedimentation coefficients were calculated using the software SEDFIT (provided by Dr. P. Schuck, National Institutes of Health) and were reduced to water and 293 K ($s_{20,w}$) by standard procedures.

2.8. Electron paramagnetic resonance

EPR (Electron Paramagnetic Resonance) spectra at X-band (9.39 GHz) were recorded by using a Bruker Elexsys E500 spectrometer equipped with a continuous-flow ^{4}He cryostat (ESR 900, Oxford Instruments) to work at variable temperatures. The perpendicular-mode EPR spectra were acquired using a field modulation of 100 kHz and 10 G, and a microwave power of 20.8 mW at 30 K. Each sample was degassed, maintained under a N_2 atmosphere and frozen immediately after addition of the metal. The ferrous ammonium sulfate and Mn(II) chloride solutions were prepared freshly, flushed with N_2 and maintained in anaerobiosis.

3. Results

3.1. X-Ray crystal structure of K. radiotolerans Dps

Purified recombinant *Kr*Dps is essentially free of Fe and Mn (≤ 0.5 Fe/12mer and ≤ 0.02 Mn/12mer) as determined by atomic absorption spectroscopy. To establish whether Mn binds at the ferroxidase center, 24 Mn(II)/12mer were added to the protein solution prior to crystallization. The X-ray quality crystals obtained after one week diffracted to 2.0 Å resolution. The *Kr*Dps X-ray structure was solved by molecular replacement using the tetramer of *Ms*Dps2 (PDB ID: 2Z90 [22]) as search model since the two sequences are 56% identical (87/155 residues).

All known Dps proteins are shell-like 12mers of identical 4-helix bundle monomers related by 23 symmetry. Thus, two types of interface are defined at the 3-fold symmetry axes. The so-called "ferritin-like" interface is formed by the N-terminal portion of the subunits and corresponds to the 3-fold interactions in the ferritin polymer with 432 symmetry. The so-called "Dps-type" interface involves the C-terminal part of the symmetry-related subunits and is present only in Dps proteins [23]. At their junction, the 3-fold symmetry related subunits create channels of two kinds that allow ions and small molecules to traverse the protein shell and reach the internal cavity. The "ferritin-like" pores are rich in aspartate residues that give rise to a negative electrostatic gradient which drives iron in and out of the cavity [24]. The "Dps-type" pores, whose precise function has not been clarified, are characterized by a marked residue variability.

In Dps proteins, the catalytic Fe(II) oxidation takes place at a bi-metallic ferroxidase center, located at the interface between 2-fold symmetry related subunits. These furnish the metal ligands as revealed by the *Li*Dps structure [23]. The two metal binding sites, called A and B, have different metal affinities. Only the higher affinity A site usually contains iron in the known Dps crystal structures. This is the case of *Li*Dps, where one iron ion is coordinated by Asp58 and Glu62 from one subunit, by His31 from the 2-fold symmetry-related one and by a water molecule that is hydrogen bonded to a second histidine (His43) from the latter subunit. This water molecule has been hypothesized to be replaced by the second iron atom and thereby give rise to the B site of a canonical bimetallic ferroxidase center [23]. The amino acids just mentioned are conserved in all Dps proteins [25,26]. In the crystal structures of *D. radiodurans* Dps2 [27] and *Bacillus brevis* Dps [28], both the A and B sites are occupied by iron, even though B site-bound iron is loosely coordinated. In *E. coli* Dps [29] and *Thermosynechococcus elongatus* Dps [30] both sites are occupied by a water molecule. This variability in iron occupancy suggests that the amino acid residues forming the second metal coordination shell influence the affinity for the metal.

The *Kr*Dps monomer displays the typical Dps 4-helix bundle fold. Superposition of the *Kr*Dps monomer structure (Fig. 1, magenta) on those of the *E. coli* Dps (*Ec*Dps) and *Ms*Dps2 monomers (blue and yellow, respectively) shows that the only differences concern the flexible parts, in particular the N-terminus. The residues forming the three long N-terminal tails are mostly hydrophobic in *Kr*Dps and give rise to two α-helical turns (α0), but are mostly hydrophilic in *Ec*Dps and *Ms*Dps2 where they assume a random coil conformation. In the *Kr*Dps 12mer, the N-terminal α0 helix of one monomer interacts with the N-terminal part of the C helix of the 3-fold symmetry related monomer (Fig. 2A) by means of mainly hydrophobic interactions which involve the α0 helix residues, Ile4, Val7, Leu12, and Ala116 and Ala112 of the C helix (Fig. 2B).

The Fo–Fc electron density map shows a strong peak due to a heavy metal at the ferroxidase center. The assignment to Mn was based on the X-ray fluorescence emission spectra of the *Kr*Dps crystal, since the most

intense peaks (at 5.88, 5.89 and 6.49 keV) correspond to those of the Mn ion (Fig. S1, panel A). Mn is coordinated at the ferroxidase center A site by Asp75, Glu79 and His48 that correspond to the three canonical Fe ligands in Dps proteins [25,26], e.g. to Asp58, Glu62 and His31 in *Li*Dps. All metal ion–ligand distances are between 2.0 and 2.2 Å. The Mn coordination geometry is bi-pyramidal (Fig. 3A). The equatorial ligands are Asp75, which ligates Mn(II) with both carboxylic oxygen atoms, His48 and a water molecule. The apical ligands are Glu79 and another water molecule (Fig. 3A). A comparison between the available Dps structures brings out that Lys45 and Asp64 play a specific role in metal binding to *Kr*Dps as they are hydrogen bonded to the metal-coordinating water molecule (data not shown). These two residues are conserved in many Dps proteins e.g. *Ec*Dps, the family prototype [29], and *Ms*Dps2 [22], but not in *T. elongatus* DpsA [31] and *D. radiodurans* Dps [32] where they are replaced by two Gln and by Lys and Gln, respectively. The *Kr*Dps metal ligands at the B site, Glu79 and His60, occupy the same position identified in *Li*Dps [23]. Interestingly, His60 is hydrogen bonded to the water molecule which furnishes one of the apical Mn ligands (HOH–NE2 distance 2.8–3.1 Å in the different monomers of the asymmetric unit). It may be hypothesized that binding of a metal at the B site displaces this water molecule and reorganizes the ferroxidase center accordingly [23].

The *Kr*Dps sequence is characterized by the unusual presence of three Trp residues (Fig. 3B). Two are conserved in all known Dps proteins, namely Trp49 and Trp158 (Trp32 and Trp144 in *Li*Dps), and are located near the ferroxidase center. The additional Trp residue, Trp56, substitutes an otherwise conserved Phe. Trp56 is hydrogen bonded via its indolic ring nitrogen atom to the carbonyl oxygen of Ile51, is placed near Trp158 (minimal distance of 4.4 Å) and forms a stacking interaction with His60 (minimal distance of 3.6 Å), a proposed metal coordinating ligand at the ferroxidase center B site. Moreover, Trp56 is near to Asn55, one of the Mn(II) ligands at the metal binding sites along the "Dps-type" interface (see below).

The structure of *Kr*Dps loaded with 24 Mn(II)/12mer shows Mn binding at sites other than the ferroxidase center. One is at the "ferritin-like" pore entrance and contains two pentacoordinated Mn
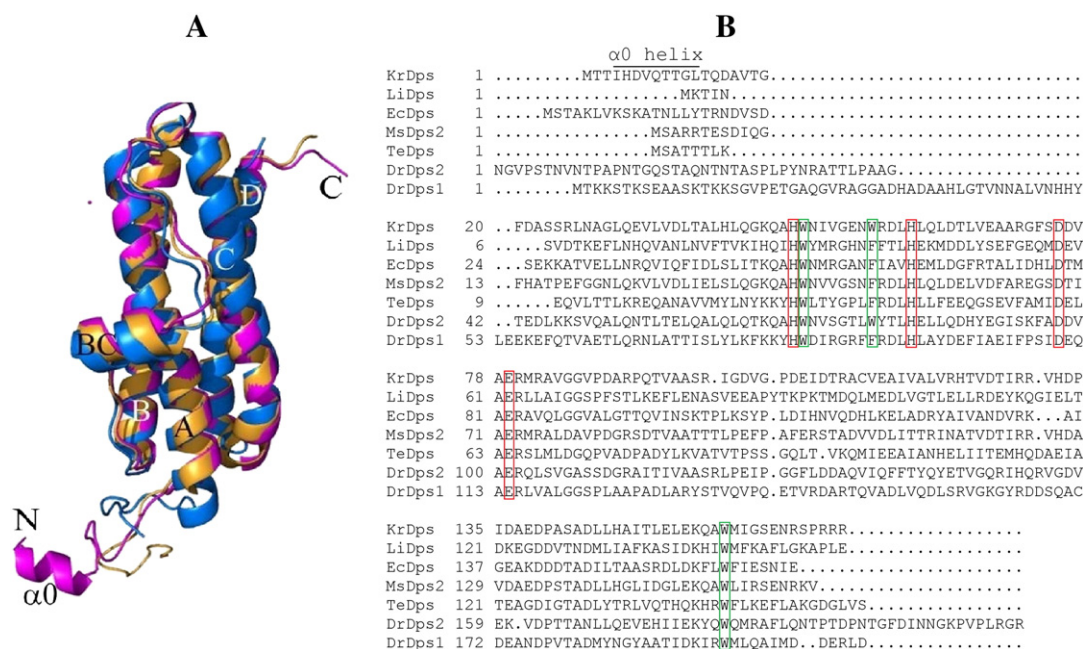

Fig. 1. Schematic representation of the *K. radiotolerans* Dps monomer structure (A) and sequence alignment of Dps proteins (B). In (A), superposition of the four antiparallel helices of *K. radiotolerans* (magenta), *E. coli* (blue) and *Mycobacterium smegmatis* Dps monomer (yellow). The additional α0 helix in *K. radiotolerans* Dps is indicated. In (B), the sequence alignment refers to the proteins from *K. radiotolerans* (*Kr*Dps; PDB ID: 4A25), *L. innocua* (*Li*Dps; PDB ID: 1QGH), *E. coli* (*Ec*Dps; PDB ID: 1DPS), *M. smegmatis* (*Ms*Dps2; PDB ID: 2Z90), *T. elongatus* (*Te*Dps; PDB ID: 2VXX) and *D. radiodurans* (*Dr*Dps1, *Dr*Dps2; PDB ID: 2C2F, 2C6R). The ferroxidase center residues are in red boxes and the Trp and Phe residues are in green boxes. The pictures were obtained with PyMol [40].
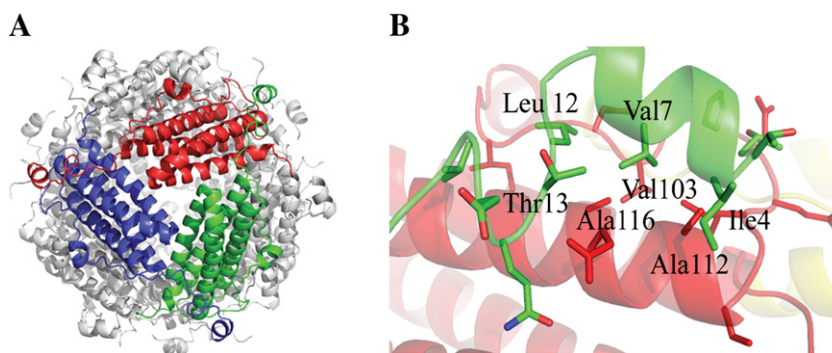
Fig. 2. View of *K. radiotolerans* Dps along the "ferritin-like" interface at the 3-fold symmetry axis (A) and detail of the interactions between the C terminal α0 helix and C helix of the 3-fold symmetry related monomer (B). Pictures were obtained with PyMol [40].

placed at a 3.4 Å distance (Fig. S1, panel B). The Mn(II) closest to the pore entrance is coordinated by the OD1 atoms of Asp144 of the 3-fold symmetry-related subunits and by two water molecules, while the second Mn(II) is coordinated by the OD2 atoms of the same residues and by two water molecules. Metal binding at the "ferritin-like" pore entrance is not unexpected, since iron and other metals enter the protein cavity through this pore, and indeed have been observed in the crystal structure of several Dps proteins [32–34]. The other Mn site is at the "Dps-type" pore entrance, a location not described before to our knowledge. Mn bound at this interface is hexa-coordinated with a typical bi-pyramidal geometry (Fig. S1, panel C) and coordination distances between 2.0 and 2.1 Å. The ligands are oxygen atoms belonging to Asn55 and Asp58 of the 3-fold symmetry related subunits.

In the Dps-like peroxide resistance protein from *Streptococcus suis* (*Ss*Dpr), one Mn ion was reported to bind at the ferroxidase center with a similar coordination as in *Kr*Dps [35]. However, no Mn binding was observed at the *Ss*Dpr "Dps-type" interface where Asn55 and Asp58, the metal ligands in *Kr*Dps, are substituted respectively by Gly and Ile.

3.2. Protein characterization in solution

The additional Trp56 in *Kr*Dps impacts on the spectroscopic properties of the protein as evidenced by a comparison of the *Kr*Dps and *Kr*Dps(W56F) UV absorbance and near-UV CD spectra (Fig. S2).

In sedimentation velocity experiments, *Kr*Dps forms a single symmetrical, homogeneous peak characterized by a weight average sedimentation coefficient, $s_{20,w}$, of 10.5 S, corresponding to a spherical molecule of ~224.5 kDa and a partial specific volume of 0.73.

3.3. Mn(II) and Fe(II) binding and incorporation properties

In Dps proteins, Fe(II) binding to the ferroxidase center, due to its location at <5 Å from one highly conserved Trp residue (e.g. Trp32 in *Li*Dps), has been followed by measuring quenching of the intrinsic protein fluorescence in anaerobiosis [36].

The same approach was applied to probe Fe(II) and Mn(II) binding at the ferroxidase center of *Kr*Dps. In a first set of titrations, 24 Fe(II)/12mer and 48 Mn(II)/12mer were added in sequence to 2 μM *Kr*Dps as purified in 4 ions/12mer increments. As reported in Fig. 4A, fluorescence intensity decreases by ~18% upon addition of ~12 Fe(II)/12mer and by a further 5% after addition of the remaining 12 Fe(II). The 5% decrease can be taken to indicate that Fe(II) binds to both the A and B sites of the ferroxidase center with different affinities, as reported for *Li*Dps on the basis of ITC experiments [36]. Binding to Asn55 and Asp58 near the "Dps-type" pores would not be sensed as the closest Trp residue, Trp56, is at about 9 Å from the A site. The subsequent addition of 48 Mn(II) results in a small fluorescence recovery. In a second set of titrations, the order of Fe and Mn additions to *Kr*Dps was reversed. Fig. 4B shows that the initial fluorescence intensity is quenched by ~10% upon addition of ~12 Mn(II)/12mer and does not change significantly when other 12 Mn(II)/12mer are added. Interestingly, the subsequent addition of 48 Fe(II)/12mer leads to further, significant quenching. The final fluorescence intensity is ~10% lower relative to the value attained upon addition of 24 Fe(II)/12mer (Fig. 4A). Based on the fluorescence data, the equilibrium dissociation constant, K_D, for Mn(II) and Fe(II) binding is respectively ≈8 μM and ≈6.5 μM, as compared to a K_D of 55 μM for Mn(II) binding to *Ss*Dpr obtained by ITC [35]. Taken together, the fluorescence titration data indicate that Mn binds only to the high affinity A site
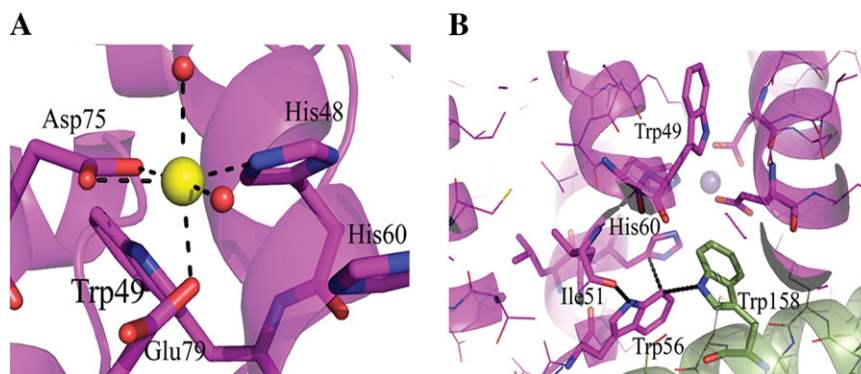

Fig. 3. Ferroxidase center in *K. radiotolerans* Dps. In (A), the Mn(II) coordinating residues are indicated in sticks, the water molecules and Mn(II) as red and yellow spheres, respectively. In (B), the position of the three Trp residues relative to the ferroxidase center is shown and the interactions of the unique Trp56 with the nearby residues are highlighted. Pictures obtained with PyMol [40].
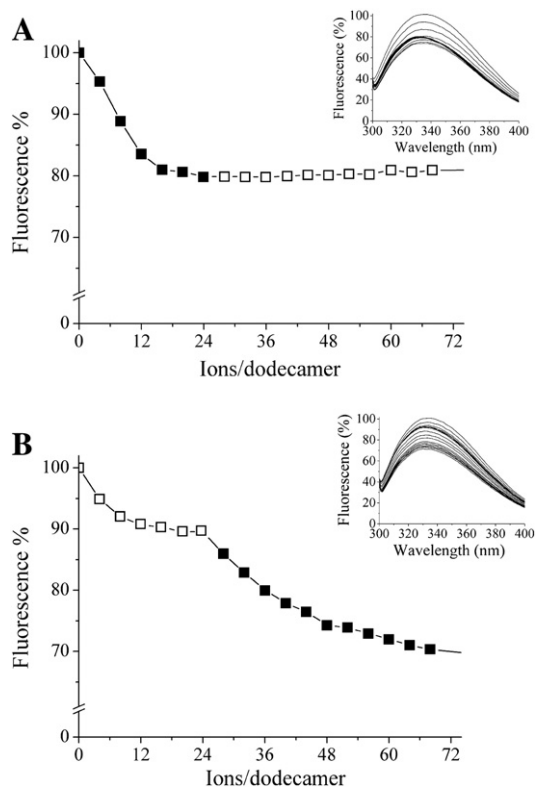
Fig. 4. Anaerobic fluorescence titration of *K. radiotolerans* Dps with Fe(II) and Mn(II). Fe(II) additions: (■), Mn(II) additions: (□). Metals were added at increments of 4 ions/12mer; in (A) Fe(II) was added before Mn(II), in (B) the order of metal addition was reversed. Protein concentration was 2 μM. The insets show the fluorescence spectra recorded at 298 K. The data points are averages of three to five measurements using 2 independent protein preparations. The standard deviation was ≤5%.

of the ferroxidase center, in accordance with the X-ray crystal structure, while Fe(II) can bind also to the low affinity B site. It appears therefore that in *Kr*Dps a hetero-metallic ferroxidase center is formed by adding 12 Mn(II) prior to 12 Fe(II).

To prove this contention, anaerobic EPR titrations with Fe(II) and Mn(II) were performed. The spectra were measured after addition of Mn(II) to 35 μM *Kr*Dps at molar ratios of 8 and 12 Mn(II)/12mer. They point to binding of the metal to *Kr*Dps with low symmetry (Figs. 5, 6A and B, spectrum 1). The spectra are characterized by many bands contributing to the signal over a wide field range as in the case of Mn(II) bound to *S. solfataricus* Dps [37]. In another set of titrations, Fe(II) and Mn(II), both at molar ratios of 12 ions/12mer, were added to *Kr*Dps in sequence. Irrespective of the order of addition of the two metals, the spectra (Fig. 6A, spectra 2 and 3) are quite similar in the g = 4.3 region (B ≈ 1500 G), but differ from the spectrum pertaining to Mn(II)-bound *Kr*Dps (Fig. 6A, spectrum 1). The changes are small, suggesting that Mn(II) is coordinated to the same site also in the presence of iron. The EPR spectrum of *Kr*Dps loaded with 12 Fe(II) and oxidized by H_2O_2 is reported in Fig. 6, spectrum 5. This spectrum (Fig. 6B) consists mainly of two signals: one at g ≈ 2 (B ≈ 3350 G) due to a radical species and a second one at g = 4.3 (B ≈ 1500 G) typical for mononuclear high-spin (S = 5/2) Fe(III) in sites of low symmetry (Fig. 6A). This g = 4.3 signal is present also in the spectra measured when the protein is incubated with 12 Mn + 12Fe/12mer, independently from the order of metal addition (Fig. 6A, spectra 2 and 3). Importantly, when both metals are bound, the width of the g = 4.3 signal increases by approximately 10 G relative to the spectrum measured with Fe(III) bound to the ferroxidase center (Fig. 6A) indicating a possible dipolar interaction between Mn(II) and Fe(III). When Mn(II) is bound to *Kr*Dps, part of
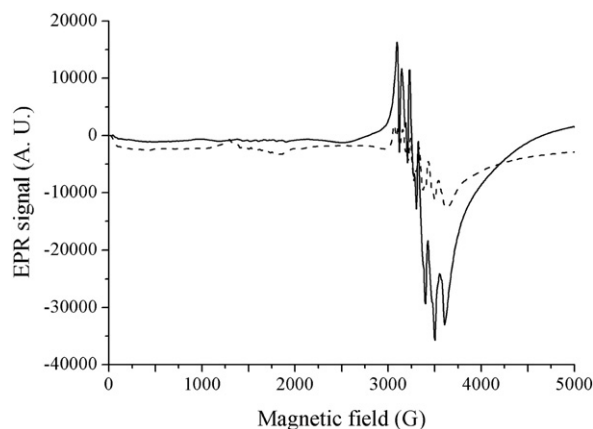

Fig. 5. Perpendicular-mode EPR spectra of *K. radiotolerans* Dps with 8 Mn(II)/12mer. Protein concentration, 35 μM. Acquisition temperature, 30 K. Mn(II)-bound protein (dashed line) and Mn(II) in buffer at equivalent concentration (solid line).

Fe(II) is oxidized prior to the addition of H_2O_2, likely due to a small O_2 leakage (see below).

The EPR data also point to differences in the development of intra-protein radicals related to the presence of the Mn–Fe center. Thus, when 12 Fe(II) are oxidized at the ferroxidase center by H_2O_2,
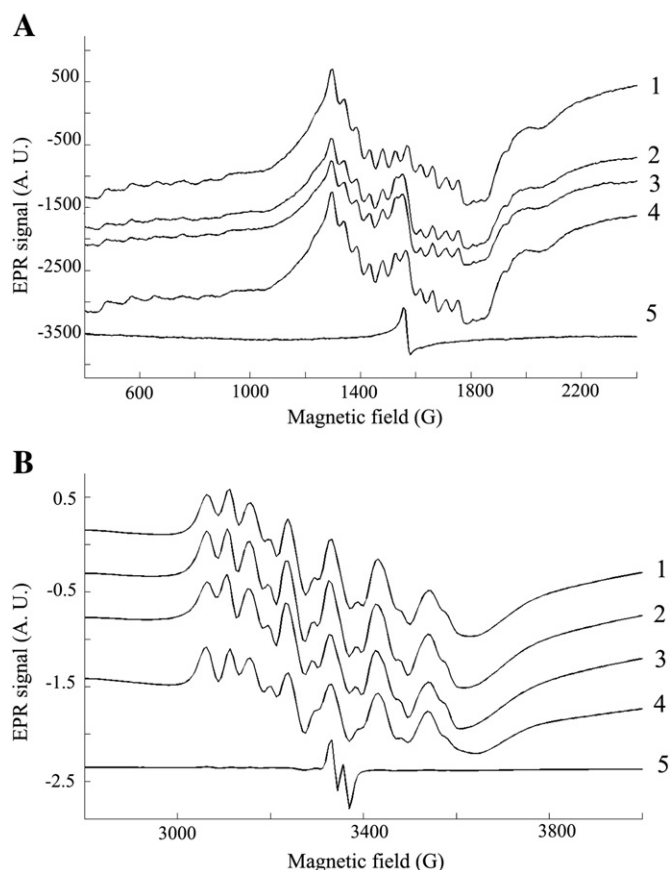

Fig. 6. Perpendicular-mode EPR spectra of *K. radiotolerans* Dps with Mn(II) and Fe(II) at molar ratios of 12 metal ions/12mer. Protein concentration, 35 μM. Acquisition temperature, 30 K. In A: Blow-up of the g = 4.3 region. *Kr*Dps with Mn(II) in anaerobiosis (spectrum 1); with Mn(II) and Fe(II) added after Mn(II) in anaerobiosis (spectrum 2); with Fe(II) and Mn(II) added after Fe(II) in anaerobiosis (spectrum 3); with Fe(II), Mn(II) and H_2O_2 (spectrum 4); with Fe(II) and H_2O_2 (spectrum 5). In B: Blow-up of the g = 2.0 region. *Kr*Dps with Mn(II) in anaerobiosis (spectrum 1); with Mn(II) and Fe(II) added after Mn(II) in anaerobiosis (spectrum 2); with Fe(II) and Mn(II) added after Fe(II) in anaerobiosis (spectrum 3); with Fe(II), Mn(II) and H_2O_2 (spectrum 4); with Fe(II) and H_2O_2 (spectrum 5).

a radical species at g = 2.0 is formed (Fig. 6B, spectrum 5). When Mn(II) is bound to the ferroxidase center, the signal attributed to the radical points to an effect of Mn(II) on the reaction mechanism (Fig. 6B, spectra 1–4).

The KrDps capacity to incorporate Fe(II) or Mn(II) inside the protein shell was assayed by sedimentation velocity after a 2 h incubation of the protein as purified in the presence of O_2 or H_2O_2 as iron oxidant. The metal ion/12mer ratio was 240, i.e. half the typical Dps iron storage capacity [24]. As expected, KrDps incorporates Fe in the presence of H_2O_2 ($s_{20,w}$ 14 S). Mn(II) incorporation does not take place irrespective of the oxidant since the $s_{20,w}$ value is unchanged (~10 S) relative to KrDps as purified (data not shown).

3.4. Redox activity of Fe(II) and Mn(II) in the presence of molecular oxygen

Fe(II) added to KrDps at 12, 24 and 48/12mer in the presence of O_2 is oxidized slowly to ferric oxy-hydroxide as in all Dps proteins [10]. The time course of Fe(II) oxidation by KrDps, monitored by the absorbance increase at 310 nm, is hyperbolic at 12 and 24 Fe/12mer and becomes sigmoidal at 48 Fe/12mer, as expected due to the onset of the ferric hydroxide nucleation reaction. Interestingly, the initial rates (determined by a linear fit of the data points from 0 to 100 s after Fe(II) addition) and the amounts of Fe(III) do not depend linearly on metal concentration. The absorbance value attained 60 min after addition of 12, 24 and 48 Fe(II)/12mer corresponds to 42 ± 1, 66 ± 3 and $86 \pm 1\%$ oxidized iron (Fig. 7A). The initial iron oxidation rate when KrDps contains 12 Fe(II)/12mer is extremely slow (4.6×10^{-8} M s^{-1}), much slower than the Fe(II) auto-oxidation rate (not shown), and increases to 25×10^{-8} M s^{-1} and 110×10^{-8} M s^{-1} respectively for KrDps with 24 and 48 Fe(II)/12mer.

The possible redox activity of Mn(II) was assayed by adding Fe(II) to KrDps pre-loaded with an equal amount of Mn(II), since Mn oxidation cannot be monitored directly by UV/visible absorbance spectroscopy. The absorbance at 310 nm was recorded after adding successively Mn(II) and Fe(II) to KrDps, each at 12 ions/12mer. The data, included in Fig. 7A, show that the initial ferroxidation rate of KrDps with 12 Mn(II) + 12 Fe(II)/12mer corresponds to 9×10^{-8} M s^{-1}, a value intermediate between those of the protein with 12 and 24 Fe(II)/12mer, indicating that A site-bound Mn(II) participates in redox cycling. Similarly, upon addition of 24 Mn(II) followed by 24 Fe(II)/12mer, the initial iron oxidation rate in air is intermediate (39×10^{-8} M s^{-1}) between those observed after addition of 24 and 48 Fe(II)/12mer. The amount of iron oxidized after 60 min is significantly higher when Mn(II) is present ($94 \pm 3\%$) relative to KrDps with just 24 Fe(II)/12mer ($66 \pm 3\%$). The presence of Mn(II) appears to be less effective when both ions are at molar ratios of 48/12mer, due to the above-mentioned contribution of the ferric hydroxide nucleation reaction.

The participation of Mn(II) in redox cycling is supported by experiments in which the order of metal addition was reversed. Fig. 7B shows the data obtained when both Mn(II) and Fe(II) are at 12 ions/12mer. When Fe(II) is added before Mn(II), the rate of iron oxidation (5.5×10^{-8} M s^{-1}) is intermediate between those observed when Mn(II) is added prior to Fe(II) (9.0×10^{-8} M s^{-1}) and that observed in the presence of 12 Fe(II) only (4.6×10^{-8} M s^{-1}). KrDps(W56F) behaves like the wt protein (data not shown). In control experiments, the rate of Fe auto-oxidation was shown to be not affected by the presence of Mn(II) at all concentrations used (not shown).

A last set of experiments was carried out to confirm the ability of Fe(II) in excess to displace Mn(II) from the A site as indicated by the fluorescence data and by the effect of Mn(II) on the ferroxidation reaction just described. Given that the affinity of Mn(II) for the A site is only marginally higher than that of Fe(II) – the estimated respective K_D values are ~8 μM and 6.5 μM – even a relatively small molar excess of Fe(II) is expected to decrease the occupancy of the A site by Mn(II). On this basis, when 12 Fe(II)/12mer are added in succession to the
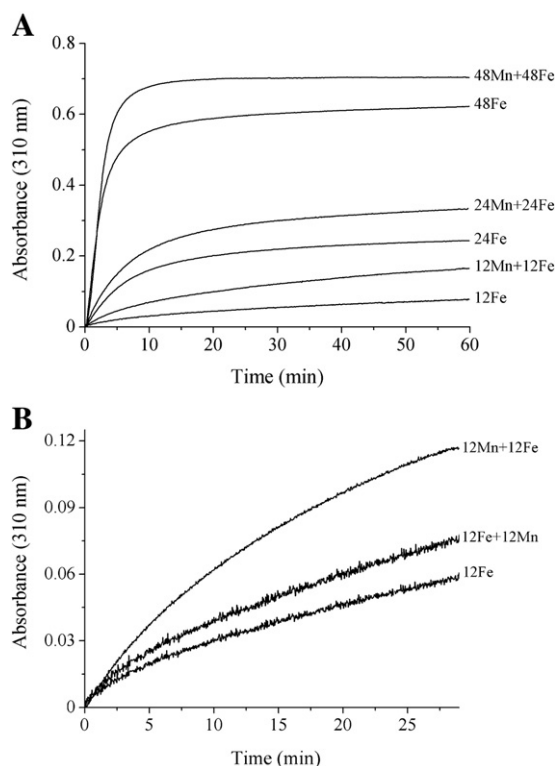
Fig. 7. Effect of Mn(II) on the kinetics of Fe(II) oxidation by O_2 in the presence of KrDps at the indicated metal ions to protein ratios. A) Protein concentration was 6 μM, temperature, 298 K. The end points of the absorbance values recorded at 310 nm, using the extinction coefficient $E_{M^{-1} cm^{-1}} = 2528$ [15] were 0.18, 0.36 and 0.72 for 12, 24 and 48 Fe(II)/12mer, respectively. B) Protein concentration was 4.6 μM; the end point of the absorbance value at 310 nm was 0.14.

same sample loaded with Mn(II), the effect of the latter metal ion on the ferroxidation reaction is expected to decrease progressively upon increase in Fe(II) concentration and eventually vanish when the amount of Fe(II) suffices to displace all the A site bound Mn(II). In fact, the rates observed upon three subsequent additions of 12 Fe/12mer to 6.5 μM KrDps containing 12 Mn/12mer are 11.4, 22.2 and 20.4×10^{-8} M s^{-1} whereas the values obtained in parallel on KrDps that does not contain Mn(II) are 5.2, 9.5, and 18.8×10^{-8} M s^{-1}.

Taken together these data indicate that A site-bound Mn participates in redox cycling only when Fe(II) is bound to the KrDps ferroxidase center B site, an assertion confirmed by the oxygraphic experiments carried out on $L.\ innocua$ Dps (see below).

The catalytic role of Mn(II) in the ferroxidation reaction by O_2 emerges clearly from Table 2, where the available data on Fe(II) binding affinities at the ferroxidase center A site and on the ferroxidation rates by O_2 of known Dps proteins are compiled.

3.5. Effect of Mn(II) on the Fe(II) oxidation reaction by hydrogen peroxide

To establish whether Mn affects the production of short-lived intra-protein radical species that trap OH$^{\bullet}$ during Fe(II) oxidation by H_2O_2, rapid mixing experiments were performed. Formation of intra-protein radical species implies that a mono electron transfer process is operative and involves aromatic residues in the neighborhood of the ferroxidase center as in LiDps and EcDps [38].

The ferroxidation reaction was followed between 350 and 700 nm by measuring the absorbance changes that occur 300 ms after the sequential mixing of 6 Fe and 3 H_2O_2 with ~17 μM KrDps. A broad band centered around 524 nm with two maxima at ~512 and 550 nm is formed 2.5 ms after mixing (Fig. 8A) as in the case of LiDps and EcDps under the same experimental conditions [38]. In EcDps these

Table 2

Fe(II) affinity for the ferroxidase center A site of Dps proteins and rate of oxidation by O_2. The apparent affinity constant for Fe(II) binding to the indicated Dps proteins was assessed by means of anaerobic fluorescence titrations (*) or ITC (°); the rates of Fe(II) oxidation were obtained at protein concentrations of ~6 μM and 25 °C.

Protein	K_A (site A) (M^{-1})	Fe(II) oxidation		pH	Ref.
		Metal/12mer	Rate ($M \times s^{-1}$)		
KrDps	$>1.5 \times 10^{5*}$	12 Fe(II)	4.6×10^{-8}	7.4	This work
	–	24 Fe(II)	25.0×10^{-8}	7.4	This work
	–	48 Fe(II)	110.0×10^{-8}	7.4	This work
		12 Mn(II) + 12 Fe(II)	9.0×10^{-8}	7.4	This work
LiDps	$>1.3 \times 10^{5*}$	12 Fe(II)	–	7.0	Ref. [36]
	$4.4 \times 10^{7°}$	24 Fe(II)	7.2×10^{-8}	7.0	Ref. [36]
	$>1.2 \times 10^{5*}$	12 Fe(II)	4.8×10^{-8}	7.4	This work
	–	24 Fe(II)	24.0×10^{-8}	7.4	This work
	–	48 Fe(II)	105.0×10^{-8}	7.4	This work
		12 Mn(II) + 12 Fe(II)	9.2×10^{-8}	7.4	This work
EcDps	–	24 Fe(II)	18.0×10^{-8}	7.0	Ref. [41]
TeDps	–	24 Fe(II)	13.6×10^{-8}	7.0	Ref. [31]

bands have been attributed to intra-protein radicals formed by Trp52. In LiDps a broad band with a maximum between 550 and 600 nm is also formed. It has been assigned to Trp32 in radical (Trp$^{\bullet}$) and in cation radical form (Trp$^{\bullet+}$), respectively [38]. In KrDps, the broad band
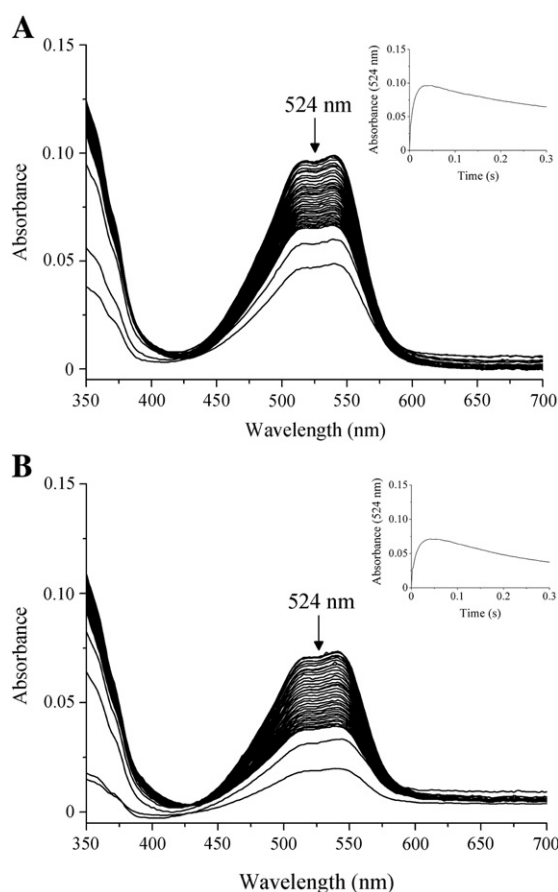
Fig. 8. Effect of Mn(II) on the Fe(II) oxidation reaction by H_2O_2. Spectral changes occurring in a KrDps solution during the first 300 ms of the oxidation reaction followed in a stopped-flow apparatus in the sequential mixing mode. In (A) KrDps was mixed with 6 Fe(II)/12mer and thereafter with 3 H_2O_2/12mer; in (B) KrDps pre-loaded with 12 Mn(II)/12mer was mixed with 6 Fe(II)/12mer and thereafter with 3 H_2O_2/12mer. Concentrations after mixing: 17 μM protein, 100 μM $FeSO_4$, 200 μM $MnCl_2$ and 50 μM H_2O_2 in 50 mM MOPS–NaOH buffer, pH 7.4 and 200 mM NaCl; temperature = 293 K. The reported spectra are taken every 6 ms. Insets report the time course of Trp$^{\bullet}$ formation assessed at 524 nm. The k values for the first phase of the reaction obtained by fitting the traces to a double-exponential time course are 118 s^{-1} (A) and 99 s^{-1} (B).

centered at 524 nm can be ascribed to the corresponding Trp49. The Trp49$^{\bullet}$ yield is $\approx 20\%$ based on the published extinction coefficient [21], a somewhat lower value relative to LiDps and EcDps [38]. The KrDps transient spectra do not show the 410 nm band attributed to a Tyr50 radical in LiDps in accordance with the presence of Val67 in the corresponding position (Fig. 1, panel B). Similarly, the 410 nm band is not formed in EcDps where Tyr50 is substituted with Arg.

In KrDps preloaded with 12 Mn(II)/12mer, the broad band attributed to Trp49$^{\bullet}$ formed upon addition of 6 Fe(II) + 3 H_2O_2/12mer has a lower intensity, corresponding to a $\approx 14\%$ yield (Fig. 8B) in line with the effect of Mn(II) on the reaction mechanism indicated by the EPR spectra depicted in Fig. 6B. No absorbance bands are detected when 12 Mn(II) + 3 H_2O_2/12mer are added to KrDps (data not shown) an indication that no intra-protein Trp$^{\bullet}$ is produced unless iron is bound at the ferroxidase center.

3.6. Mn(II) and Fe(II) binding to L. innocua Dps as a model system

To establish the generality of the Mn(II) binding and oxidation capacity of the Dps ferroxidase center, the well characterized LiDps was used under the same conditions employed for KrDps albeit without NaCl in the buffer. The two Dps proteins behave very similarly as shown in Fig. S3, panels A–E. Oxygraphic assays were also performed to detect O_2 consumption upon addition of Fe(II) to LiDps in the presence and absence of Mn(II). Importantly, no O_2 is consumed when Mn(II) is added to the buffer in the absence of protein. In contrast, O_2 consumption takes place at 95 $nmol^{-1}$ when Fe(II) is present (Fig. S4). In accordance with the spectrophotometric assays, O_2 consumption is accelerated when KrDps contains both Mn and Fe.

4. Discussion

Mn(II) binding at the ferroxidase center of Dps proteins and its participation in redox cycling during Fe(II) oxidation are of interest from different perspectives. In radiation-resistant bacteria, whose cytoplasm is especially rich in Mn(II) and poor in Fe(II), it provides a likely molecular mechanism for the protective role exerted by Mn under oxidative stress conditions. From a general viewpoint it brings out that the Dps ferroxidase center can operate also in a transient hetero-bimetallic state, with Mn(II) at the A site and Fe(II) at the B one, a condition where functional differences between the two sites are manifested. The metal bound to the high affinity A site, be it Fe(II) or Mn(II), appears to play a catalytic role during ferroxidation, whereas the B site-bound Fe(II) acts as a substrate that leaves the site after oxidation and can be substituted by incoming Fe(II). Importantly, A site-bound Mn(II) does not undergo redox processes unless the B site contains Fe(II).

The crystallographic structure of Mn(II)-containing KrDps clearly reveals that Mn(II) binds at the high affinity A site, whereas the B site remains metal-free (Fig. 3A), even though the metal added (24 Mn(II)/12mer) suffices to saturate both sites at the concentrations used for crystallization. The structural reason for the higher affinity of Mn(II) for the A site relative to iron is not known. The A site-bound Mn(II) is hexa-coordinated: Asp75, Glu79 and His48 correspond to the canonical Fe(II) binding residues and furnish four ligands, while the other two ligands are provided by water molecules. One H_2O is anchored in position by Lys45 and Asp64. A comparison with Mn(II) binding at the structurally related ferroxidase centers is in order. In the ferroxidase center of S. suis Dpr, differences in the Mn(II) ligands relative to KrDps are apparent. In particular, His59 (corresponding to His60, a B site metal ligand in KrDps) does not contribute to metal binding due to the lack of the water molecule (W2011-C) that bridges Mn(II) and His60 in KrDps. Moreover, Glu78 is unable to provide a mono-dentate Mn(II) ligand at the B site as it is slightly tilted away from the ferroxidase center, whereas the corresponding Glu79 is a bi-dentate ligand in the structures of Mn(II)-bound KrDps. The binuclear ferroxidase

center of the dodecameric Dps-like protein from *S. solfataricus*, is buried within the four-helix bundle of each monomer as in bacterioferritins and mammalian ferritins, and is able to bind both iron and manganese. Each metal is coordinated by Glu, His, and one water molecule, with the two metals bridged by a glutamic acid carboxylate [14]. A hetero-nuclear Mn–Fe cofactor has been described also in the so-called class I ribonucleotide reductases (RNRs), like *C. trachomatis* RNR [13], where it takes the place of the typical Fe–Fe cofactor. The overall configuration of the Mn–Fe center and of the homo-metallic iron one in conventional RNRs is alike, an observation that accounts for the binding of two Mn(II) in *E. coli* RNR (PDB ID: 3N37). In this protein, bound Mn(II) is hexa-coordinated: one Mn(II) ion is ligated by His, a water molecule and three Glu residues (one provides a bi-dentate interaction), while the other Mn(II) is coordinated by His, Asp, three Glu residues and a water molecule [39].

*Kr*Dps possesses other Mn(II) binding sites at the "ferritin-like" and "Dps-type" interfaces (Fig. S1, panels B and C). Metal binding at the latter position has not been observed in other Dps proteins likely due to the variability of the residues lining this interface. In fact, the *Kr*Dps Mn(II) binding residues Asn55 and Asp58 are conserved in *Ms*Dps2 [22], but not in *Li*Dps [23], *Ec*Dps [29] and *Ss*Dpr [35]. In turn, Mn(II) bound at the *Kr*Dps "Dps-type" pore entrance suggests that *Kr*Dps may use these pores for metal passage towards the ferroxidase center. Furthermore, *Kr*Dps contains an unusual Trp residue (Trp56) which substitutes the otherwise conserved Phe and is located at less than 4 Å from the ferroxidase center B site and at 9 Å from Mn bound at the "Dps-type" interface. However, given the similar behavior of the wt protein and of the *Kr*Dps(W56F) mutant, Trp56 is unlikely to play a significant role in metal binding.

In full agreement with the crystallographic data, which show that Mn(II) binding at the ferroxidase center involves only the A sites, the anaerobic fluorescence titrations indicate binding of 12 Mn(II)/12mer with high affinity, in contrast with the binding of 24 Fe(II)/12mer at both the A and B sites (Fig. 4A and B). In turn, when Mn(II) and Fe(II) are added to *Kr*Dps in succession at 12 ions/12mer, this characteristic can lead to formation of a hetero-nuclear ferroxidase center with Mn(II) bound at the A site and Fe(II) at the B site. Mn(II) and Fe(II) bind to the A site with similar affinities such that Mn(II) is displaced by Fe(II) in molar excess as indicated by the observed ferroxidation rates when successive amounts of Fe(II) are added to *Kr*Dps in the presence or absence of Mn(II) at the ferroxidase A site and by the fluorescence titrations (Fig. 4).

In the ferroxidation reaction, the Mn–Fe hetero-nuclear center behaves differently from the canonical Fe–Fe one as the presence of Mn(II) renders Fe(II) oxidation by O₂ more effective (Fig. 7A, B). This situation recalls the higher efficiency of the *C. trachomatis* RNR Mn–Fe cluster relative to the typical Fe–Fe cofactor in providing the oxidation equivalent needed to initiate catalysis [13]. In Mn–Fe–*Kr*Dps, oxidation of B-site bound Fe(II) is faster than in the Fe–Fe containing protein and is complete after 60 min in air. This finding clearly indicates that Mn(II) undergoes redox cycling and favors Fe(II) oxidation at the B site. In the absence of Mn(II), Fe(II) oxidation by O₂ is not complete under the same conditions and, intriguingly, the amount of Fe(III) formed does not correspond to the total amount of Fe(II), but rather to that of B site-bound Fe(II). It appears therefore that A site-bound Fe(II) and Mn(II) behave alike in that they favor Fe(II) oxidation at the B site.

EPR experiments prove Mn(II) binding to the *Kr*Dps ferroxidase center. Moreover, they indicate formation of a hetero-metallic cofactor when Mn and Fe are added sequentially in equal amounts to the protein sample and are oxidized by H₂O₂. Thus, when iron is added to *Kr*Dps pre-loaded with Mn(II), there is an approximately 10 G increase of the signal in the g = 4.3 region with respect to the protein loaded with iron only (Fig. 6A). These data point to the occurrence of a dipolar interaction between the two metals. The nature of this weak interaction is in accordance with formation of a transient hetero-nuclear Mn(II)–

Fe(III) center wherefrom Fe(III) bound to the B site can move to the protein cavity (see below). In the protein loaded with 12 Mn(II)/12mer and 12 Fe(II)/12mer, the fact that part of the Fe(II) is oxidized also in absence of H₂O₂ is likely due to an oxygen leak, consistent with the increase in Fe(II) oxidation rate by O₂ due to bound Mn(II) depicted in Fig. 7.

In mechanistic terms, these findings, which apply also to *Li*Dps (Fig. S3, panel C), suggest different roles for the A and B sites during ferroxidation by molecular oxygen. A site-bound Fe(II) or Mn(II) participates in redox cycling, does not leave the A site, and hence has a mere catalytic function. In contrast, the B site-bound Fe(II) behaves like a substrate that, once oxidized, can move into the protein cavity and give rise to ferric oxy-hydroxide nuclei.

Iron oxidation by H₂O₂ in the presence of Dps proteins leads to the complete two-electron reduction of H₂O₂ to water, but is known to involve transfer of single electrons and the consequent formation of transient intra-protein radical species. These act as a short-lived radical trap that dissipates free electrons and limits the release of OH⁻ in solution and the ensuing oxidative DNA damage. Radical formation involves the conserved Trp and Tyr residues located near the ferroxidase center [38].

The Mn(II) redox cycling activity in the ferroxidation reaction when H₂O₂ is the oxidant is envisaged to entail the following steps:

1) A site-bound Mn(II) and B site-bound Fe(II) provide the electron pair for the reduction of H₂O₂ to water with formation of the transient Fe(II)–Mn(III) intermediate detected in the EPR experiments:

$$H_2O_2 + 2H^+ + Mn^{+2} + Fe^{+2} = 2H_2O + Mn^{+3} + Fe^{+3}$$
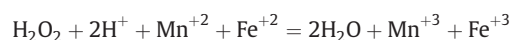
2) thereafter, oxidized Fe(III) leaves the B site and gives rise to the nucleation process in the cavity, while Mn(III) undergoes a second redox reaction by acquiring an electron from the nearby Trp49 residue through a short-range electron transfer; this process regenerates Mn(II) and forms the Trp⁻ radical species detected in the stopped-flow experiments presented in Fig. 8:

$$Mn^{+3} + Trp49 = Mn^{+2} + Trp49^•$$
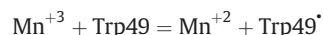
3) thereafter, another Fe(II) binds to the B site, reduces Trp49⁻ to Trp49, and leaves the site as Fe(III), giving rise to the nucleation process in the protein cavity. In this reaction mechanism, two Fe(II) are oxidized by one H₂O₂ molecule.

When O₂ acts as Fe(II) oxidant, since H₂O₂ is an intermediate reaction [36], the Mn(II) redox cycling activity can be envisaged to entail the following steps:
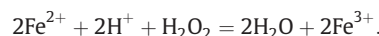
1) A site-bound Mn(II) and B site-bound Fe(II) provide the electron pair for the reduction of O₂ to hydrogen peroxide:

$$O_2 + 2H^+ + Mn^{+2} + Fe^{+2} = H_2O_2 + Mn^{+3} + Fe^{+3}$$
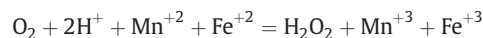
2) oxidation of another Fe(II) leads to regeneration of Mn^{2+}:

$$Mn^{+3} + Fe^{2+} = Mn^{2+} + Fe^{3+}$$
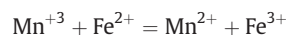
3) hydrogen peroxide is reduced by the mechanism described above:

$$2Fe^{2+} + 2H^+ + H_2O_2 = 2H_2O + 2Fe^{3+}.$$

The data on *Li*Dps extend these observations and indicate that A site-bound Mn(II) abolishes Tyr⁻ formation and decreases Trp⁻ formation (Fig. S3, panel E). In *Kr*Dps, the relevant Tyr residue (Tyr50 in *Li*Dps) is substituted by a valine (Fig. 1, panel B) and mono-electron transfer involves only Trp49, the conserved tryptophan localized near the catalytic site (Fig. 8A). When *Kr*Dps contains the hetero-nuclear Mn–Fe center, the amount of Trp⁻ decreases (Fig. 8B) and is nil in *Kr*Dps containing

only Mn(II) (data not shown), a further indication of the absence of redox processes under this condition. The oxygraphic assays carried out on *Li*Dps (Fig. S4) require to be recalled in this connection as they provide convincing evidence that A site-bound Mn(II) does not undergo redox processes unless Fe(II) is at the B site. The EPR spectra support this contention since the $g = 2$ signal, characteristic of radical species formation, is not present when *Kr*Dps is loaded with 12 Mn(II)/12mer (Fig. 6B). The similarity of all the Mn(II) effects in *Kr*Dps and in *Li*Dps, the family prototype, points to their generality.

At variance with Fe, Mn is not incorporated in the *Kr*Dps cavity as shown by the $s_{20,w}$ value which is unchanged, relative to apo-*Kr*Dps, after incubation with 240 Mn(II)/12mer in the presence of O_2 or H_2O_2. In contrast, $s_{20,w}$ increases from ~10 S to ~14 S in *Kr*Dps incubated with 240 Fe(II)/12mer. It appears therefore that Mn(II) acts as a catalytic element in the reduction of O_2 and H_2O_2 without forming a manganese oxide or a manganese–iron oxide core within the protein shell.

5. Conclusions

The present data disclose that in Dps proteins metals bound at the ferroxidase center A and B sites have different functional roles. The high affinity A site can bind Fe(II) or Mn(II) which act as catalysts during ferroxidation, whereas the low affinity B site binds only Fe(II) that migrates towards the protein cavity after each ferroxidation cycle and thus behaves like a substrate. In more general terms, the capacity of Dps proteins to bind Mn(II) and use it to carry out both iron oxidation and H_2O_2 consumption can be of physiological relevance in radiation-resistant bacteria that can survive exposure to strong oxidants, prolonged desiccation and other DNA-damaging agents. In these bacteria, the catalytic role of Mn(II) bound at the Dps ferroxidase center is expected to be significant given the high cytosolic Mn concentration and the increased Dps expression under ionizing conditions.

Protein Data Bank accession codes

The *Kr*Dps coordinates have been deposited in the Protein Data Bank with the PDB ID code 4A25 and with the structure factors code r4A25sf.

Acknowledgements

Appendix A. Supplementary data

Supplementary data to this article can be found online at http://dx.doi.org/10.1016/j.bbagen.2013.02.003.

References

[1] A.G. McEvan, New insights into the protective effect of manganese against oxidative stress, Mol. Microbiol. 72 (2009) 812–814, http://10.1111/j.1365-2958.2009.06700.

[2] F.S. Archibald, I. Fridovich, Manganese and defences against oxygen toxicity in *Lactobacillus plantarum*, J. Bacteriol. 145 (1981) 442–451, (http://www.ncbi.nlm.nih.gov/pmc/articles/PMC217292/).

[3] F.S. Archibald, I. Fridovich, The scavenging of superoxide radical by manganous complexes *in vitro*, Arch. Biochem. Biophys. 214 (1982) 452–463, http://10.1016/0003-9861(82)90049-2.

[4] F.S. Ezra, D.S. Lucas, R.V. Mustacich, A.F. Russell, Phosphorus-31 and carbon-13 nuclear magnetic resonance studies of anaerobic glucose metabolism and lactate transport in *Staphylococcus aureus* cells, Biochemistry 22 (1983) 3841–3849, http://10.1021/bi00285a020.

[5] F.S. Ezra, D.S. Lucas, A.F. Russell, ^{31}P-NMR and ESR studies of the oxidation states of manganese in *Staphylococcus aureus*, Biochim. Biophys. Acta 803 (1984) 90–94, http://10.1016/0167-4889(84)90059-4.

[6] F. Fiorini, S. Stefanini, P. Valenti, E. Chiancone, D. De Biase, Transcription of the *Listeria monocytogenes fri* gene is growth-phase dependent and is repressed directly by Fur, the ferric uptake regulator, Gene 410 (2008) 113–121, http://10.1016/j.gene.2007.12.007.

[7] H. Chen, R. Wu, G. Xu, X. Fang, X. Qiu, H. Guo, B. Tian, Y. Hua, DR2539 is a novel DtxR-like regulator of Mn/Fe ion homeostasis and antioxidant enzyme in *Deinococcus radiodurans*, Biochem. Biophys. Res. Commun. 396 (2010) 413–418, http://10.1016/j.bbrc.2010.04.106.

[8] A. Anjem, S. Varghese, J.A. Imlay, Manganese import is a key element of the OxyR response to hydrogen peroxide in *Escherichia coli*, Mol. Microbiol. 72 (2009) 844–858, http://10.1111/j.1365-2958.2009.06699.x.

[9] A. Ilari, M.C. Latella, P. Ceci, F. Ribacchi, M. Su, L. Giangiacomo, S. Stefanini, N.D. Chasteen, E. Chiancone, The unusual intersubunit ferroxidase center of *Listeria innocua* Dps is required for hydrogen peroxide detoxification but not for iron uptake. A study with site-specific mutants, Biochemistry 44 (2005) 5579–5587, http://10.1021/bi050005e.

[10] F. Pacello, P. Ceci, S. Ammendola, P. Pasquali, E. Chiancone, A. Battistoni, Periplasmic Cu, Zn superoxide dismutase and cytoplasmic Dps concur in protecting *Salmonella enterica* serovar Typhimurium from extracellular reactive oxygen species, Biochim. Biophys. Acta 1780 (2008) 226–232, http://10.1016/j.bbagen.2007.12.001.

[11] M.J. Daly, E.K. Gaidamakova, V.Y. Matrosova, A. Vasilenko, M. Zhai, A. Venkateswaran, M. Hess, M.V. Omelchenko, H.M. Kostandarithes, K.S. Makarova, L.P. Wackett, J.K. Fredrickson, D. Ghosal, Accumulation of Mn(II) in *Deinococcus radiodurans* facilitates gamma-radiation resistance, Science 306 (2004) 1025–1028, http://10.1126/science.1103185.

[12] M.J. Daly, A new perspective on radiation resistance based on *Deinococcus radiodurans*, Nat. Rev. Microbiol. 7 (2009) 237–245, http://10.1038/nrmicro2073.

[13] N. Voevodskaya, F. Lendzian, O. Sanganas, A. Grundmeier, A. Gräslund, M. Haumann, Redox intermediates of the Mn–Fe site in subunit R2 of *Chlamydia trachomatis* ribonucleotide reductase. An X-ray absorption and EPR study, J. Biol. Chem. 284 (2009) 4555–4566, http://10.1016/j.jbc.M807190200.

[14] G.H. Gauss, P. Benas, B. Wiedenheft, M. Young, T. Douglas, C.M. Lawrence, Structure of the Dps-like protein from *Sulfolobus solfataricus* reveals a bacterioferritin-like dimetal binding site within a Dps-like dodecameric assembly, Biochemistry 45 (2006) 10815–10827, http://10.1021/bi060782u.

[15] M. Bozzi, G. Mignogna, S. Stefanini, D. Barra, C. Longhi, P. Valenti, E. Chiancone, A novel non-heme iron-binding ferritin related to the DNA binding proteins of the Dps family in *Listeria innocua*, J. Biol. Chem. 272 (1997) 3259–3265, http://10.1074/jbc.272.6.3259.

[16] S.C. Gill, P.H. von Hippel, Calculation of protein extinction coefficients from amino acid sequence data, Anal. Biochem. 182 (1989) 319–326, http://10.1016/0003-2697(89)90602-7.

[17] Z. Otwinowski, W. Minor, Processing of X-ray diffraction data collected in oscillation mode, Methods Enzymol. 276 (1997) 307–326, http://10.1016/S0076-6879(97)76066-X.

[18] A. Vagin, A. Teplyakov, Molecular replacement with MOLREP, Acta Crystallogr. Sect. D: Biol. Crystallogr. 66 (2010) 22–25, http://10.1107/S0907444909042589.

[19] M.D. Winn, G.N. Murshudov, M.Z. Papiz, Macromolecular TLS refinement in REFMAC at moderate resolutions, Methods Enzymol. 374 (2003) 300–321, http://10.1016/S0076-6879(03)74014-2.

[20] P. Emsley, K. Cowtan, COOT: model-building tools for molecular graphics, Acta Crystallogr. Sect. D: Biol. Crystallogr. D60 (2004) 2126–2132, http://10.1107/S0907444904019158.

[21] S. Solar, N. Getof, S. Parminder, D.A. Armstrong, A. Singh, Oxidation of tryptophan and N-methylindole by $N_3\bullet$, $Br_2\bullet-$, and $(SCN)_2\bullet-$ radicals in light- and heavy-water solutions: a pulse radiolysis study, J. Phys. Chem. 95 (1991) 3639–3643, http://10.1021/j100162a038.

[22] S. Roy, R. Saraswathi, D. Chatterji, M. Vijayan, Structural studies on the second *Mycobacterium smegmatis* Dps invariant and variable features of structure, assembly and function, J. Mol. Biol. 25 (2008) 948–959, http://10.1016/j.jmb.2007.10.023.

[23] A. Ilari, S. Stefanini, E. Chiancone, D. Tsernoglou, The dodecameric ferritin from *Listeria innocua* contains a novel intersubunit iron-binding site, Nat. Struct. Mol. Biol. 7 (2000) 38–43, http://10.1038/71236.

[24] P. Ceci, G. Di Cecca, M. Falconi, F. Oteri, C. Zamparelli, E. Chiancone, Effect of the charge distribution along the "ferritin-like" pores of the proteins from the Dps family on the iron incorporation process, J. Biol. Inorg. Chem. 16 (2011) 869–880, http://10.1007/s00775-011-0784-9.

[25] S. Stefanini, P. Ceci, M. Ardini, A. Ilari, DNA-binding proteins from starved cells (Dps proteins), in: A. Messerschmidt (Ed.), Handbook of Metalloproteins, J. Wiley & Sons, Chichester (UK), 2010, pp. 1–10, http://10.1002/0470028637.met258.

[26] E. Chiancone, P. Ceci, The multifaceted capacity of Dps proteins to combat bacterial stress conditions. Detoxification of iron and hydrogen peroxide and DNA binding, Biochim. Biophys. Acta 1800 (2010) 798–805, http://10.1016/j.bbagen.2010.01.013.

[27] M.G. Cuypers, E.P. Mitchell, C.V. Romão, S.M. McSweney, The crystal structure of the Dps from *Deinococcus radiodurans* reveals an unusual pore profile with a non-specific metal binding site, J. Mol. Biol. 371 (2007) 789–799, http://10.1016/j.jmb.2006.11.032.

[28] B. Ren, G. Tibbelin, T. Kajino, O. Asami, R. Ladenstein, The multi-layered structure of Dps with a novel di-nuclear ferroxidase center, J. Mol. Biol. 329 (2003) 467–477, http://10.1016/S0022-2836(03)00466-2.

[29] R.A. Grant, D.J. Filman, S.E. Finkel, R. Kolter, J.M. Hogle, The crystal structure of Dps, a ferritin homolog that binds and protects DNA, Nat. Struct. Mol. Biol. 5 (1998) 294–303, http://10.1038/nsb0498-294.

[30] S. Franceschini, P. Ceci, F. Alaleona, E. Chiancone, A. Ilari, Antioxidant Dps protein from the thermophilic cyanobacterium *Thermosynechococcus elongatus*, FEBS J. 273 (2006) 4913–4928, http://10.1111/j.1742-4658.2006.05490.x.

[31] F. Alaleona, S. Franceschini, P. Ceci, A. Ilari, E. Chiancone, *Thermosynechoccus elongatus* DpsA binds Zn(II) at a unique three histidine-containing ferroxidase center and utilizes O_2 as iron oxidant with very high efficiency, unlike the typical Dps proteins, FEBS J. 277 (2010) 903–917, http://10.1111/j.1742-4658.2009.07532.x.

[32] S.G. Kim, G. Bhattacharyya, A. Grove, Y.H. Lee, Crystal structure of Dps-1, a functionally distinct Dps protein from *Deinococcus radiodurans*, J. Mol. Biol. 361 (2006) 105–114, http://10.1016/j.jmb.2006.06.010.

[33] T.J. Stilman, M. Upadhyay, V.A. Norte, S.E. Sedelnikova, M. Carradus, S. Tzokov, P.A. Bullough, C.A. Shearman, M.J. Gasson, C.H. Williams, P.J. Artymiuk, J. Green, The crystal structures of *Lactococcus lactis* MG1363 Dps proteins reveal the presence of an N-terminal helix that is required for DNA binding, Mol. Microbiol. 57 (2005) 1101–1112, http://10.1111/j.1365-2958.2005.04757.x.

[34] A. Kauko, S. Haataja, A.T. Pulliainen, J. Finne, A.C. Papageorgiou, Crystal structure of *Streptococcus suis* Dps-like peroxide resistance protein Dpr: implications for iron incorporation, J. Mol. Biol. 338 (2004) 547–558, http://10.1016/j.jmb.2004.03.009.

[35] T. Haikarainen, A. Thanassoulas, P. Stavros, G. Nounesis, S. Haataja, A.C. Papageorgiou, Structural and thermodynamic characterization of metal ion binding in *Streptococcus suis* Dpr, J. Mol. Biol. 405 (2011) 448–460, http://10.1016/j.jmb.2010.10.058.

[36] M. Su, S. Cavallo, S. Stefanini, E. Chiancone, N.D. Chasteen, The so-called *Listeria innocua* ferritin is a Dps protein. Iron incorporation, detoxification, and DNA protection properties, Biochemistry 44 (2005) 5572–5578, http://10.1021/bi0472705.

[37] J.A. Hayden, M.P. Hendrich, EPR spectroscopy and catalase activity of manganese-bound DNA-binding protein from nutrient starved cells, J. Biol. Inorg. Chem. 15 (2010) 729–736, http://10.1007/s00775-010-0640-3.

[38] G. Bellapadrona, M. Ardini, P. Ceci, S. Stefanini, E. Chiancone, Dps proteins prevent Fenton-mediated oxidative damage by trapping hydroxyl radicals within the protein shell, Free Radic. Biol. Med. 48 (2010) 292–297, http://10.1016/j.freeradbiomed.2009.10.053.

[39] A.K. Boal, J.A. Cotruvo Jr., J. Stubbe, A.C. Rosenzweig, Structural basis for activation of class Ib ribonucleotide reductase, Science 329 (2010) 1526–1530, http://10.1126/science.1190187.

[40] W.L. DeLano, The PyMOL Molecular Graphics System, DeLano Scientific, San Carlos (CA), 2002.

[41] G. Zhao, P. Ceci, A. Ilari, L. Giangiacomo, T.M. Laue, E. Chiancone, N.D. Chasteen, Iron and hydrogen peroxide detoxification properties of DNA-binding protein from starved cells, J. Biol. Chem. 277 (2002) 27689–27696, http://10.1074/j be.M202094200.